Spiraling solitons: A continuum model for dynamical phyllotaxis of physical systems

Cristiano Nisoli

Theoretical Division and Center for Nonlinear Studies, Los Alamos National Laboratory, Los Alamos, New Mexico 87545, USA
(Received 30 April 2009; published 11 August 2009)

A protean topological soliton has recently been shown to emerge in systems of repulsive particles in cylindrical geometries, whose statics is described by the number-theoretical objects of phyllotaxis. Here, we present a minimal and local continuum model that can explain many of the features of the phyllotactic soliton, such as locked speed, screw shift, energy transport, and—for Wigner crystal on a nanotube—charge transport. The treatment is general and should apply to other spiraling systems. Unlike, e.g., sine-Gordon-like systems, our soliton can exist between nondegenerate structures and its dynamics extends to the domains it separates; we also predict pulses, both static and dynamic. Applications include charge transport in Wigner Crystals on nanotubes or *A*- to *B*-DNA transitions.

I. INTRODUCTION

The topological soliton, the moving domain wall between degenerate structures, ubiquitously populates systems of discrete symmetry, most notably the Ising model, and appears at different scales and in many realms of physics [1]: in mechanical or electrical apparatus [1–3], superconducting Josephson junctions [4], nonperturbative theory of quantum tunneling [5], and particle physics (e.g., Yang-Mills monopoles and instantons [6], sigma model lumps, and skyrmions [7]).

Recently Nisoli *et al.* [8] discovered a novel kind of topological soliton in systems of repulsive particles whose degenerate statics is dictated by the intricate and fascinating number-theoretical laws of phyllotaxis. As the phenomena they describe are purely geometrical in origin, one would expect this kind of "phyllotactic" soliton to play a role in many different physical systems at different scales, wherever repulsive particles in cylindrical geometries are present [8].

Physically, the problem appears to be highly nonlocal, as energy and momentum are not confined inside the soliton but flows through it between the rotating domains it separates (see below). Yet, in this paper we show that a minimal, local, and continuum model for the phyllotactic soliton that subsumes the effect of the kinetic energy of the domains into a modification of the potential energy in the familiar equivalent Newtonian problem [5] can correctly predict its speed, the transfer of energy between boundaries, the observed shift in screw angle, and the charge-density variations, and it can classify its rather complicated zoology.

II. FROM LEVITOV'S TO DYNAMICAL PHYLLOTAXIS

In the early 1990s, while studying vortices in layered superconductors, Levitov [9] showed that a system of repulsive particles on a long cylinder presents a rich degenerate set of ground states; these can be labeled by number-theoretical objects, the Farey classes, which arise in phyllotaxis, the study of dispositions of leaves on a stem, and other self-organized structures in botany [10]. While it is still debated whether Levitov's model is the best suited to explain botanical phyllotaxis, it certainly imported the same mathematical structures into the description of a variety of physical systems. Already, phyllotactic patterns had been seen or predicted outside the domain of botany [11], in polypeptide chains [12], cells of Bénard convection [13], or vortex lattices in superconductors [9].

Dynamical cactus

Recently Nisoli *et al.* [8] showed numerically and experimentally that physical systems whose statics is dictated by phyllotaxis can access dynamics in ways unknown in botany. They investigated the statics and the dynamics of a prototypical phyllotactic system, the dynamical cactus of Fig. 1, and found that, while its statics faithfully reproduce phyllotaxis, its dynamics reveal new physics beyond pattern formation. In particular, the set of linear excitations contains classical rotons and maxons; in the nonlinear regime, both dynamical simulations and experiments revealed a novel highly structured family of topological solitons that can change identity upon collision and posses a very rich dynamics [8]. Unlike other topological solitons, the phyllotactic one separates domains of different dynamics; these domains can store kinetic energy while rotating around the axis of the dynamical cactus; energy and momentum flow across the soliton. Moreover, as those domains are different, the kinks among them have different shapes, characteristic speeds, and behaviors under collision. In some simple cases the dynamics of the soliton can be modeled heuristically via conservation laws, and certain observables—such as its speed—can be computed in this way. A more general and complete approach would obviously be desirable.

The dynamical cactus, a simple phyllotactic system depicted in Fig. 1, consists of repulsive massive objects holonomically constrained on rings rotating around a fixed axis: let $a=L/N$ be the distance between consecutive rings for a cylinder of length L and radius R containing N objects, θ_i be the angular coordinate of the ith particle, and $\omega_i=\theta_i-\theta_{i-1}$ be the angular shift between consecutive rings. The total potential energy for unit length is then
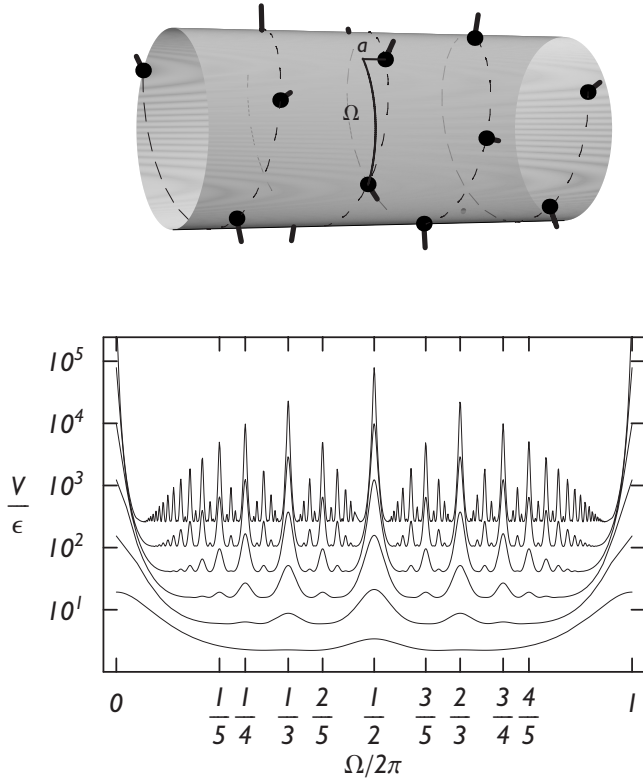
FIG. 1. Top: the dynamical cactus, repulsive particles (here dipoles), on the surface of a cylinder. a is the distance between consecutive rings and Ω is their angular shift. The dashed line is the so-called "generative spiral" [10]. Bottom: for a dipole-dipole interaction, energy V versus screw angle Ω (semilogarithmic plot) for halving values of the parameter a/R starting from 0.5 (lowest line), in arbitrary units ϵ.

$$V = \frac{1}{2L} \sum_{i \neq j} U(\theta_i - \theta_j), \tag{1}$$

where U is any long-ranged repulsive interaction that makes the sum extensive and well behaved, such as a dipole-dipole or a screened Coulomb.

It has been shown that stable structures correspond to spiraling lattices [8], where each ring is shifted from the previous by the same screw angle $\omega_i = \Omega$. The energy of spiraling structures as a function of Ω is reported in Fig. 1 for different values of a/R: as a/R decreases, more and more commensurate spirals become energetically costly, independent of the repulsive interaction used; for every j, there is a value of a/R low enough such that any commensurate spiral of screw angle $2\pi i/j$ with i, j relatively prime, becomes a local maximum, as particles facing after j rings become nearest neighbors in the real space. The minima also become more nearly degenerate as the density increases since, for angles incommensurate to π, each particle is embedded in a nearly uniform incommensurately smeared background formed by the other particles [8].

One-dimensional degenerate systems are entropically unstable against domain wall formation [14]. Kinks between stable spirals were found numerically and experimentally

[8]. Numerically, it was proved that these kinks can propagate along the axis of the cylinder. Experimentally, the dynamical cactus was observed expelling a higher-energy domain by propagating its kink.

As discussed in Ref. [8] such axial motion of a kink between two domains of different helical angles confronts a dilemma: helical phase is unwound from one domain at a different rate than it is wound up by the other. Numerical simulations show that the moving domain wall solves this problem by placing adjacent domains into relative rotation (see supplementary materials in Ref. [8] for an animation).

Detailed dynamical simulations reveal a complex zoology of solitons, along with an extraordinarily rich phenomenology: kinks of different species merge, decay, change identity upon collision, and decompose at high temperature into a sea of constituent lattice particles.

III. CONTINUUM MODEL

A. Lagrangian

To describe domain walls between degenerate structures of the dynamical cactus, we propose a minimal continuum model. First, in the continuum limit, we promote the site index i to a continuum variable: $ia \rightarrow z$, $\theta_i \rightarrow \theta(z)$, the screw angle is now $\omega_i \rightarrow \omega(z) \equiv a\partial_z\theta$ (later we will just assume $a = 1$). A spiral corresponds to $\omega(z) = \partial_z\theta(z) = \text{const}$. A kink corresponds, in the ω, z diagram, to a transition between two constant values.

We seek a model that is local and returns the right energy when the system is in a stable configuration. To express the cost in bridging two stable domains, we introduce a generalized rigidity κ. We thus propose the (linear density of) Lagrangian as

$$\mathcal{L} = \frac{1}{2}I\dot{\theta}^2 - V(\partial_z\theta) - \frac{\kappa}{2}(\partial_z^2\theta)^2. \tag{2}$$

The first term is the kinetic energy ($I \equiv \mathcal{I}a^{-1}$, with being the moment of inertia of a ring). The second accounts locally for the potential energy, so that the Hamiltonian from Eq. (2) returns the right energy for a static (or uniformly rotating) stable spiral like those observed experimentally. The last term, the lowest-order correction allowed both in the field θ and in its derivatives, conveys the rigidity toward spatial variations of the screw angle and ensures that a kink always corresponds to a positive-energy excitation.

The Euler-Lagrangian equation of motion follows directly from Eq. (2) as

$$I\partial_t^2\theta = \partial_z V'(\partial_z\theta) - \kappa\partial_z^4\theta \tag{3}$$

and corresponds to the conservation of the density angular momentum $I\partial_t\theta$, where the density of current of angular momentum is $V'(\partial_z\theta) - \kappa\partial_z^3\theta$ (V' is the derivative of V with respect to its argument and represents the local torque).

In the following we will prove that, whatever is the precise form of the actual potential V, and the geometric parameters of the problem, there exist solitonic solutions of Eq. (3) between local minima of V. We will show how to derive many qualitative and quantitative results by reducing the

problem to an equivalent one-dimensional Newtonian equation, as customary for these kinds of problems [5], yet with a significant twist.

B. Equivalent Newtonian picture

We seek a uniformly translating solution of Eq. (3)

$$\theta = \theta(z - vt) + wt, \tag{4}$$

where the constant w accounts for angular rotation invariance, reflects the underlying transverse structure in our system (which is lacking in Klein-Gordon-like systems) and is the source of much of the unique physics. By defining $s = z - vt$, we find $\partial_t^2 \theta = v^2 d^2\theta/ds^2$, which leads to the *equivalent Newtonian equation* [5]

$$\kappa \frac{d^2\omega}{ds^2} = -\Phi'(\omega) \tag{5}$$

whose *equivalent potential* Φ is given by

$$\Phi(\omega) = \tfrac{1}{2}v^2 I(\omega - \tilde{\omega})^2 - V(\omega). \tag{6}$$

$\tilde{\omega}$ is a constant that is sometimes useful to redefine as $\tilde{\omega} \equiv \tau/(Iv^2)$ in terms of τ, which has the dimension of a torque. We will find that in studying static solitons it is easier to use τ, while for dynamical ones $\tilde{\omega}$ is preferable.

In the equivalent Newtonian picture a soliton corresponds to a trajectory $\omega(s)$ of a point particle that starts with zero kinetic energy on the top of a maximum of $\Phi(\omega)$ and, in an infinite amount of "time" s, reaches the neighboring maximum of equal height as detailed in Fig. 2. A similar treatment applies to Klein-Gordon-like solitons and tunneling problems [5,14]. Yet the presence of an extra quadratic term translates in completely different physics and accounts for the dynamics of the domains.

C. Shift from stability

Because of the quadratic term $\tfrac{1}{2}v^2 I(\omega - \tilde{\omega})^2$ in the expression of Φ, and unlike the Klein-Gordon-like soliton, our soliton in general does not connect ω_1, ω_2, which are local minima of V; rather it goes from $\bar{\omega}_1 = \omega_1 + \delta_1$ to $\bar{\omega}_2 = \omega_2 + \delta_2$, bridging spirals whose screw angle is slightly shifted away from stability, with the shift increasing with the speed of the kink (Fig. 2).

We find then a most interesting result: *a moving soliton cannot connect two stable structures*. At most, it can bridge a stable spiral ω_1 with one shifted away from equilibrium $\bar{\omega}_2 = \omega_2 + \delta_2$, if we choose $\tilde{\omega} = \omega_1$, but only if $V(\omega_1) < V(\omega_2)$.

These shifts away from stability were observed in dynamical simulations [integrating the full equation of motion for the discrete system of particles interacting via Eq. (1)] in the form of precursor waves propagating at the speed of sound in front of the soliton as in Fig. 3. They correspond to the physically intuitive fact that, in order to move, the kink needs a torque to propel it.

Clearly, static solitons ($v = 0$) can bridge stable spirals if these are degenerate, i.e., $V(\omega_1) = V(\omega_2)$. On the other hand, if two domains are degenerate, and are connected by a moving soliton, they *both* need to be shifted.
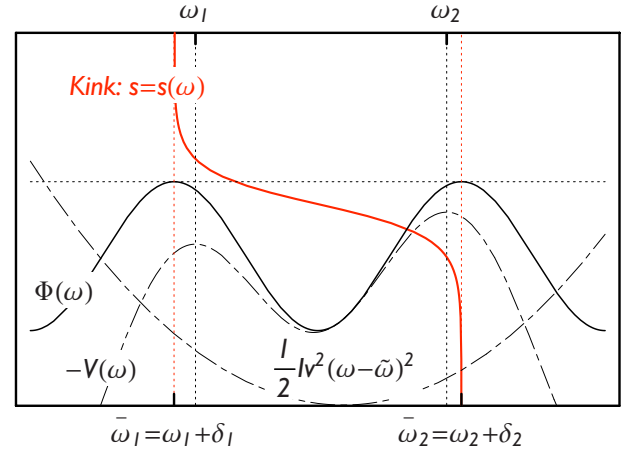

FIG. 2. (Color online) The equivalent Newtonian picture, standard for Klein-Gordon-like solitons or for tunneling problems [5]: a soliton is a solution of Eq. (5) that corresponds to a trajectory $\omega(s)$ [red solid line (light gray)] of a point particle that starts and ends in two equally valued maxima [horizontal dotted red lines (light gray)] of the equivalent potential energy $\Phi(\omega) = \tfrac{1}{2}v^2 I(\omega - \tilde{\omega})^2 - V(\omega)$ (black solid line). As the kinetic energy must be zero on those maxima, it takes the Newtonian trajectory an infinite amount of time s (i.e., "time" in the Newtonian picture, space in the soliton picture) to reach the "top of the hill" with asymptotic speed equal to zero [5]. Unlike the Klein-Gordon-like case, the presence of the quadratic term $\tfrac{1}{2}v^2 I(\omega - \tilde{\omega})^2$ (dashed line), which accounts for the kinetic energy of the domains, slightly shifts the asymptotic value of the kinks (red dotted lines) away from stable static structures ω_1, ω_2 (black dotted lines), the minima of the real potential energy $V(\omega)$ (dashed line). Instead, the soliton connects spirals of angle $\bar{\omega}_1 = \omega_1 + \delta_1$, $\bar{\omega}_2 = \omega_2 + \delta_2$, which in general are not stable structures of V. The extra quadratic term also allows solitons among nondegenerate configurations and brings the speed of the soliton v into the picture. [Everything is in arbitrary units. The soliton is obtained by numerical integration of the Eq. (5) using the energy profile portrayed in the figure.]

D. Boundary conditions

The conditions of existence of a soliton between the asymptotic domains $\bar{\omega}_1, \bar{\omega}_2$ are

$$\Phi'(\bar{\omega}_1) = \Phi'(\bar{\omega}_2) = 0,$$

$$\Phi(\bar{\omega}_1) = \Phi(\bar{\omega}_2). \tag{7}$$

Now, from Eq. (4), we obtain the expression of the angular velocity for a soliton of speed v,

$$\dot{\theta}(s) = -v\omega(s) + w, \tag{8}$$

which implies that, in general, as the soliton travels along the axis, *one or both of its two domains must be set into rotation and at different angular velocities*. As mentioned, this rotation of the domains is indeed observed in dynamical simulations [8] as the mechanism with which the soliton unwinds and rewinds spirals of different gaining angles.
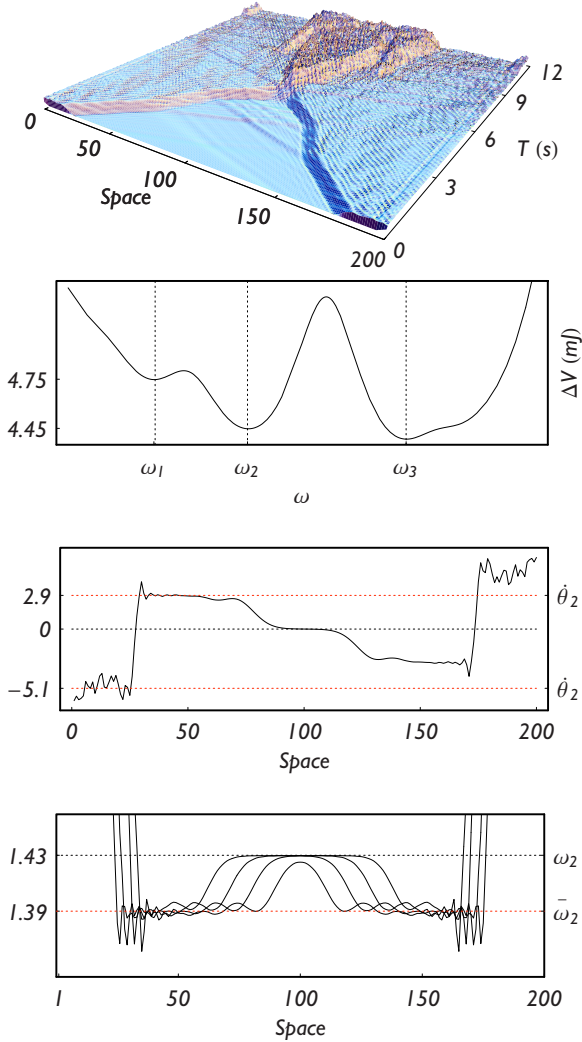
FIG. 3. (Color online) Dynamical simulation for the collision or conversion of two solitons, emitted from free boundaries of a dynamical cactus. Top panel: screw angle vs space (in number of rings) and time (in seconds); note the elastic wave preceding the soliton. Second panel: energy per particle (mJ) vs screw angle (rad) for our system ($\omega_1 = 1.79$ rad, $\omega_2 = 1.43$ rad, $\omega_3 = 2.40$ rad); the two kinks—before collision—connect a high (inner: ω_1) to a low (outer: ω_2) energy domain; after collision a low (inner: ω_3) to a high (outer: ω_2). Third panel: angular speed (s^{-1}) vs space at a given time: the speed of the soliton can be extracted as $v = \Delta\dot\theta/\Delta\omega = 22.1$ s^{-1} (predicted: 23.4 s^{-1}). Fourth panel: the precursor; plot of the screw angle vs space at different times while the soliton and its preceding wave advance. The amplitude δ_1 of the precursor is predicted via Eq. (13) as $\delta_1 = \omega_1 - \bar\omega_1 = -0.043$ rad, in excellent agreement with numerical observations. The simulation uses the experimental density and the magnetic interaction as in Ref. [8]. (See supplementary materials in Ref. [8] for an animation.)

Unlike Klein-Gordon-like one-dimensional topological solitons, which separate essentially equivalent static domains and can travel at any subsonic speed [14], we see that phyllotactic domain walls instead separate regions of different dynamics: energy and angular momentum *flow through* the topological soliton as it moves, rather than being concentrated in it; as mentioned above, this was used to show heu-

ristically that its speed v is tightly controlled by energy-momentum conservation, phase matching at the interface, and boundary conditions [8]. We will show how a more precise version of those heuristic formulas can be deduced within the framework of our continuum model and in a more general fashion.

The angular speed of rotation of the domains depends on the parameter w, which along with $\tilde\omega$ is a constant to be determined. On the other hand, we can show that energy conservation constrains w to $\tilde\omega$. In fact, when the two domains are shifted from equilibrium, and thus subjected to a torque, energy flows through the boundaries of the system as the domains rotate. By imposing no energy accumulation in the kink, we fix w in Eq. (4) in the following way: the power entering the system at the asymptotic boundaries can easily be deduced via the Noether theorem to be

$$j_{\pm\infty} = -\lim_{s\to\pm\infty} V'(\omega(s))\dot\theta(s), \qquad (9)$$

which is, not surprisingly, the torque times the angular speed. By requiring $j_{+\infty} = j_{-\infty}$ an equation for $w, \tilde\omega$ is found as

$$w = v(\bar\omega_1 + \bar\omega_2 - \tilde\omega), \qquad (10)$$

which will come in hand in many practical cases.

IV. ZOOLOGY

A. Static kinks

Let us explore static kinks first. Equations (7) reduce to

$$\tau = V'(\bar\omega_1) = V'(\bar\omega_2),$$
$$\tau(\bar\omega_1 - \bar\omega_2) = V(\bar\omega_1) - V(\bar\omega_2). \qquad (11)$$

The first of the two Eqs. (11) tell us that τ is a torque applied at the asymptotic boundaries of the system, while the second shows that no torque is necessary if the topological soliton connects degenerate structures, as we anticipated. Unlike topological solitons of the Klein-Gordon class, here *static kinks are allowed between nondegenerate domains through an applied torque* that shifts the two structures out of the minima of V.

B. Solitons moving between nondegenerate domains

Unlike the Klein-Gordon-like Lagrangian, our Lagrangian is not invariant under Poincaré group. Our traveling soliton is not just a boost of the static one, as it is clear from Fig. 2. In particular the shifts of the domains from stability increase with the speed v. By expanding $V(\omega)$ around its local minima and using Eq. (6), one finds easily that small shifts are proportional to the square of the speed of the soliton, or $\delta_1, \delta_2 \propto v^2$.

Let us consider a particular case of practical importance. Kinks between nondegenerate structures can sometimes be found in the experimental settings, because of static friction, after having annealed mechanically the cactus with free boundaries. If a small perturbation is given, enough to overcome that friction, the dynamical cactus will expel the

higher-energy domains by propagating the kink along the axis [8]. Figure 3 reports a dynamical simulation of this case obtained by integrating the full equation of motion for the discrete system of particles whose interaction is given in Eq. (1).

Let us show how our continuum model can reproduce a soliton between nondegenerate minima and provide quantitative predictions. Free boundaries imply $j_{\pm\infty}=0$: since $v \neq 0$, V' cannot be zero on both boundaries, as we saw before, nor can the angular speed of rotation of the domains be. The only possible free boundaries solution is that one has $V'=0$ on one side and $\partial_t\theta=0$ on the other. Hence the soliton must connect, say, $\bar{\omega}_2=\omega_2$ to $\bar{\omega}_1=\omega_1+\delta_1$, with $V(\omega_2)<V(\omega_1)$, which fixes $\tilde{\omega}=\omega_2=\bar{\omega}_2$. Equations (7) then fix the speed of the soliton as

$$v_k^2 = \frac{2\Delta\bar{V}}{I\Delta\bar{\omega}^2} \qquad (12)$$

with $\Delta\bar{V}=V(\bar{\omega}_1)-V(\bar{\omega}_2)$ and $\Delta\bar{\omega}=\bar{\omega}_2-\bar{\omega}_1$ (in this particular case, $\omega_2=\bar{\omega}_2$). Equation (12) corrects an earlier formula found heuristically via energy conservation, which neglected the shifts [8]. From the angular velocities of rotation of the domains in the dynamical simulation (Fig. 3, third panel), a speed of 22.1 s^{-1} can be extracted and compared with the value 23.4 s^{-1} predicted by Eq. (12): the small discrepancy is likely due to energy dissipation into phonons—a known effect for solitons in discrete systems.

From Eq. (10), we find $w=v\bar{\omega}_2$ which together with Eq. (8) implies that the region of lower energy rotates uniformly, while that of higher energy, which is shifted, remains still: since there is no energy flow through the boundaries, the kink transforms the potential-energy difference between the two domains into the kinetic energy of rotation—and vice versa, depending on its direction of propagation. (Only propagation toward lower potential energies was observed experimentally [8].)

By expanding V around ω_1, $V\simeq\frac{1}{2}Ic_1^2(\omega-\omega_1)^2$, where c_1 is the speed of sound in the spiral of angle ω_1, we obtain an approximate expression for the shift of the screw angle in the region of higher energy

$$\frac{\delta_1}{\Delta\omega} = \frac{v^2/c_1^2}{1-v^2/c_1^2} \qquad (13)$$

that clearly holds for $v\ll c_1$. As the system is prepared in a stable nonshifted configuration of angle ω_1, a precursor in front of the soliton propagates to accommodate the shift δ_1, as it was seen yet not understood in the dynamical simulation reported in Fig. 3 [8]. Equation (13) applied to the experimentally measured $V(\omega)$ employed in the simulation predicts a shift $\delta_1=-0.043$ rad, which fits the results of the simulation well (Fig. 3, last panel).

We will not deal here with collisions between solitons. Yet, even without the knowledge of the precise form of V, a few considerations can be made on asymptotic states of the collision depicted in Fig. 3: the domains beyond the approaching pair of kink-antikink rotate with opposite angular velocity $\dot{\theta}=v\Delta\omega$, with v given by Eq. (12). After the colli-
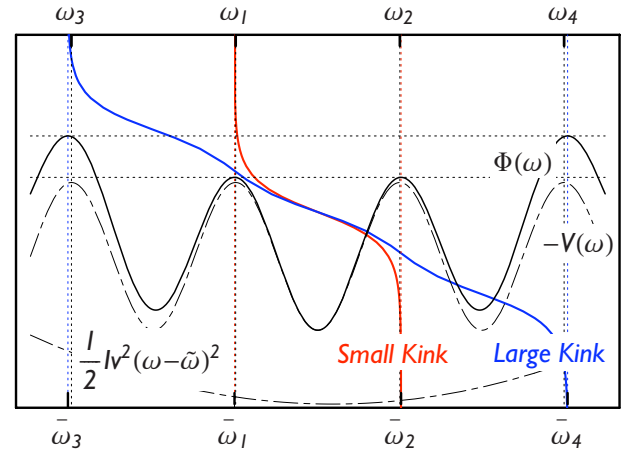

FIG. 4. (Color online) Equivalent Newtonian diagram (see caption of Fig. 2 for explanation) for symmetric solitons between degenerate spirals. As the quadratic term raises all the maxima of $-V(\omega)$, solitons with the same speed but connecting different domains are possible under different applied torques. The smallest kink [solid red line (light gray)] and a larger kink [solid blue line (dark gray)] are shown.

sion v changes sign, and so must $\Delta\omega$. The infinitely long domains cannot invert angular velocity instantaneously: the emerging asymptotic configuration must be that of a pair of different kink-antikinks, connecting the old asymptotic domain with a different nearest neighbor, hence the collision metamorphosis already discussed in Ref. [8].

C. Solitons moving between degenerate domains

To investigate the degenerate case, typical of dynamical phyllotaxis of high R/a ratios (Fig. 1), we consider for simplicity the potential V of Fig. 4; degeneracy requires now that $\tilde{\omega}=(\omega_1+\omega_2)/2$, and if the potential is symmetric as in the figure, both boundaries are equally shifted in opposite directions and subjected to a torque of opposite sign and equal intensity [from Eqs. (7)]

$$|\tau| = \frac{I}{2}v^2(\bar{\omega}_2-\bar{\omega}_1). \qquad (14)$$

Exactly, as in the case of the boosted Klein-Gordon-like one, our symmetric soliton becomes shorter as v increases (Fig. 2), although via a completely different mechanism. In the Klein-Gordon-like soliton, shortening is a consequence of relativistic contraction of the Poincaré group. Instead, in our case, v raises the difference between the maxima of Φ and the minima among them. That means higher "kinetic energy" in the "valley" of Φ for the equivalent trajectory, thus higher values of $d\omega/ds$, and hence a shorter soliton.

Equations (8)–(10) tell us that the two domains rotate in opposite direction with angular velocity of the same intensity

$$|\dot{\theta}| = v(\bar{\omega}_2-\bar{\omega}_1). \qquad (15)$$

In practice, the system acts like a mechanical inverter of rotation that transmits a power $\tau\dot{\theta}=Iv^3\Delta\bar{\omega}^2/2$ along the tube. For any given velocity, many solitons between degenerate
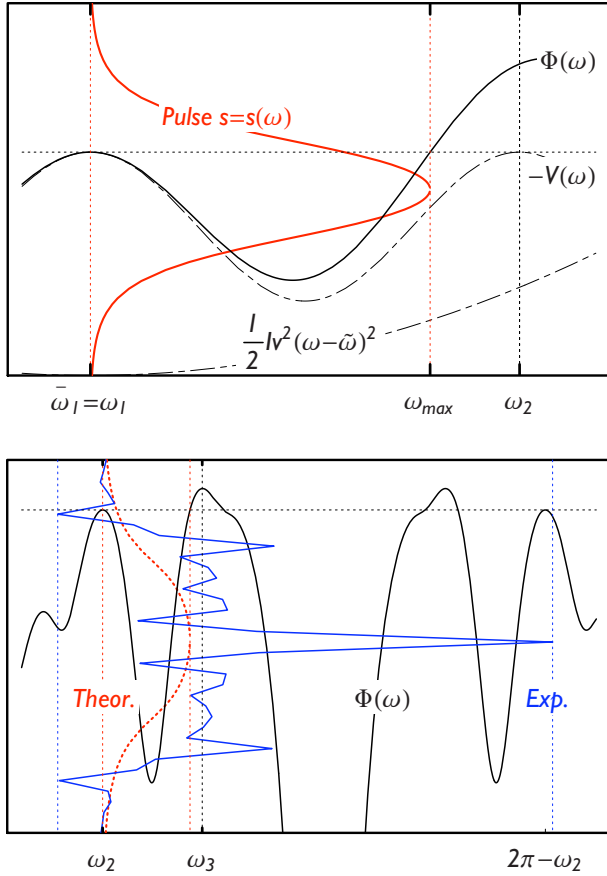
FIG. 5. (Color online) Equivalent Newtonian diagram (see caption of Fig. 2 for explanation) for pulses. Top: a traveling pulse among degenerate structures is possible because the nonzero speed v raises the maximum of Φ. Bottom: theoretical [red dashed (light gray)] and experimental [blue solid (dark gray)] frozen-in pulse on the measured energy curve of the dynamical cactus [8].

structures are allowed, corresponding to different applied torques, as in Fig. 4.

D. Pulses: Propagating and frozen in

The equation of motion also predicts pulses, both dynamic and static (frozen in). The top panel of Fig. 5 shows the pulse soliton in the equivalent Newtonian picture as a trajectory falling from a local maximum of Φ, say ω_1, and coming back to it without reaching the neighboring $\bar{\omega}_2$ because of a higher potential barrier.

Clearly, pulses possess less inertia than kinks since only the region occupied by the pulse rotates during propagation. Theory suggests that these pulses should be able to propagate with free boundaries and that no applied torque is necessary—although solutions corresponding to different boundary conditions, and hence applied torque, can be found as well by choosing $\tilde{\omega} \neq \omega_1$.

Let us consider pulses in stable structures and thus $\tilde{\omega} = \omega_1$. When $v > c$, (the speed of sound in the spiral of angle ω_1) then ω_1 becomes a minimum for Φ and we obtain a solution that oscillates around ω_1: *the speed of sound is the*

upper limit for the velocity of the pulse soliton. As v decreases three things can happen.

If $V(\omega_1) < V(\omega_2)$, then pulses exist for $v_k < v < c$, with v_k given in Eq. (12). As v approaches from above the critical value v_k, the pulse asymptotically stretches to a pair of kink and antikink between domains ω_1 and $\bar{\omega}_2$, placed at infinite distance from each other, traveling at the same speed in the same direction. If $V(\omega_1) = V(\omega_2)$, the situation is the same as above, yet the critical value for asymptotic stretch into kink and antikink is $v = 0$. If $V(\omega_1) > V(\omega_2)$, we have a pulse soliton for every value of $v < c$. As v goes to zero, the pulse freezes into a static one. Hence, in the absence of torque at the boundaries, our theory predicts that *static pulses* can exist in every structure, except in the lowest-energy one.

These frozen-in kinks that were indeed observed experimentally (but not understood) in higher-energy spirals perhaps arise from a kink-antikink symmetric collision [15] at the interplay with friction. Figure 5, bottom, shows in solid blue (dark gray) line the data from the experimental apparatus, along with our frozen-in soliton calculated within our continuum model, and the dotted red (light gray) line shows the data for the energy $\Phi = V$ (solid black line) empirically measured in the experimental apparatus.

V. AXIALLY UNCONSTRAINED CASE

We have since now considered only an axially constrained case where the repulsive particles were allowed to rotate around an angular coordinate, but not to translate along the axis. Nonlocal optimization via a structural genetic algorithm has shown that the more general case of axially unconstrained particles on a cylindrical surface reproduces the same fundamental statics of the axially constrained one, i.e., the same spiraling lattices [15]. Numerical simulations have also shown kinks propagating among the spirals [15]. The most significant difference with the axially constrained case is a drop in density in the region of the kink to locally relieve the mismatch. If these particles were charged, the drop in density would endow the soliton with a net charge: the phyllotactic soliton could function as a charge carrier. In fact, Wigner crystals of electrons on large semiconducting tubes are candidate environments for the phyllotactic soliton at nanoscale as discussed in Ref. [8]. A crystal pinned by the corrugation potential and/or impurities will not slide along the tube under a weak enough external field.

A simple extension of the continuum model can easily incorporate variations in the linear density and allow investigation of the possibility of charge transport by the phyllotactic soliton. We rescale the interaction as

$$V \rightarrow \left(\frac{\lambda}{\lambda_o}\right)^2 V, \qquad (16)$$

where λ is the linear density in the presence of axial displacement, whereas $\lambda_o = N/L$. Let $\zeta = dz/a$ be the relative axial displacement; then, if $\partial_z \zeta \ll 1$ we have $\lambda/\lambda_o = 1/(1 + \partial_z \zeta)$. The new Lagrangian reads

$$\mathcal{L} = \frac{1}{2}I\dot{\theta}^2 + \frac{1}{2}IR^{-2}\dot{\zeta}^2 - \frac{V(\partial_z\theta)}{(1+\partial_z\zeta)^2} - \frac{\kappa}{2}(\partial_z^2\theta)^2. \quad (17)$$

To gain insight regarding the shape of the soliton, we restrict ourselves to the simpler static case with no applied torque. By variation in the Lagrangian in Eq. (17), one obtains

$$\frac{d^2\omega}{dz^2} = -\frac{V'(\omega)}{1+\partial_z\zeta},$$

$$\partial_z\left[\frac{2V(\omega)}{(1+\partial_z\zeta)^3}\right] = 0, \quad (18)$$

which, along with the normalization condition for λ, returns the density of a static soliton (kink or pulse) as a function of $\omega(z)$,

$$\frac{\lambda(z)}{\lambda_o} = \left(\frac{V_o}{V[\bar{\omega}(z)]}\right)^{2/3}. \quad (19)$$

Here V_o is the asymptotic value of V at the boundaries. The static kink $\bar{\omega}(z)$ can be found as the solution of the equivalent Newtonian equation (5) with potential

$$\Phi(\omega) = -V_o^{2/3}V(\omega)^{1/3}. \quad (20)$$

Now, $V^{1/3}$ and V have the same set of local minima, and the same ordering among their values: *the extension to axial displacements does not alter any of the conditions for the existence of kink and pulse solitons*, at least for the static case.

Equation (19) implies, as expected, a drop in density similar to a dark soliton in the region of the kink, and thus, for a crystal of charges, a net charge. In particular, the higher the potential barrier between the two domains, the lower the density at the center of the kink. Also, from Eq. (20) we can see that allowing an extra degree of freedom makes the kink longer. In practice the kink can take advantage of density reduction to relax the potential barrier between the two domains and can thus be longer. All of this is detailed in Fig. 6, where the solitons for both the axially constrained and unconstrained cases (along its variation in density) are reported for the same interaction among particles. Analogous considerations apply to static pulses. The case of the axially unconstrained traveling soliton is more complicated and will not be treated here.

VI. CONCLUSION

We have introduced a minimal, local, and continuum model for the phyllotactic soliton and showed that its predictions are in excellent agreement with numerical data, that it provides a tool to calculate otherwise elusive quantities, such as charge transport, energy-momentum flow, speed of the soliton, and angular velocities, and that it could be used in the future to develop its thermodynamics.
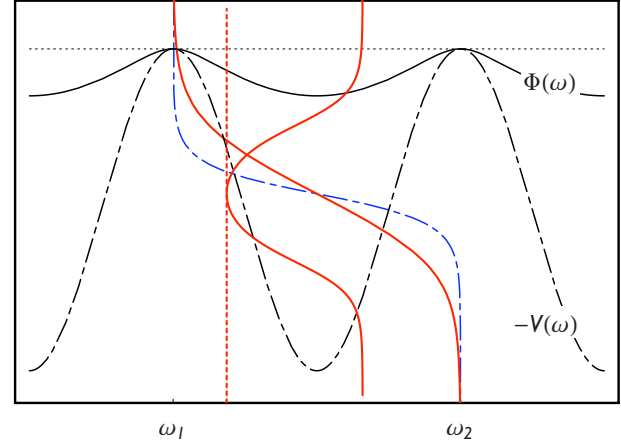

FIG. 6. (Color online) Equivalent Newtonian diagram for both axially constrained and unconstrained soliton. In blue dashed (dark gray) curve, the axially constrained soliton among the stable structures ω_1, ω_2 is shown. The two red solid curves (light gray) depict the soliton in the axially unconstrained case, which is longer, and its corresponding drop in density λ.

Our continuum model should be applicable to many different physical systems. As discussed in Ref. [8], dynamical phyllotaxis is purely geometrical in origin, and thus the rich phenomenology of the phyllotactic soliton could appear across nearly every field of physics. Indeed phyllotactic domain walls have already been seen, but not recognized, in simulations [16] of cooled ion beams [17] where the system self-organizes into concentric cylindrical shells. Colloidal particles on a cylindrical substrate provide a highly damped version [18], and polystyrene particles in air (as used to investigate [19] the Kosterlitz, Thouless, Halperin, Nelson, and Young theory of two-dimensional melting [20]) have reasonably low damping and long-range interaction.

Yet it should be noticed that our model has a range of application much wider than pure dynamical phyllotaxis. Domain walls in any spiraling system whose energy depends on the screw angle of the spirals, which manifest different stable spiraling structures and where a generalized rigidity can be reasonably introduced to describe transitions between different spirals, should be described by such formalism. Kinks in spiraling proteins and in particular transitions between *A*- and *B*-DNA might be approachable this way.

[1] M. Remoissenet, *Waves Called Solitons* (Springer-Verlag, Berlin, 1999).

[2] A. C. Scott, Am. J. Phys. **37**, 52 (1969).

[3] K. Nakajima, T. Yamashita, and Y. Onodera, J. Appl. Phys. **45**, 3141 (1974).

[4] A. V. Ustinov, Physica D **123**, 315 (1998).

[5] H. Kleinert, *Path Integrals* (World Scientific, Singapore, 1995).

[6] A. Actor, Rev. Mod. Phys. **51**, 461 (1979).

[7] N. Manton and P. Sutcliffe, *Topological Solitons* (Cambridge University Press, Cambridge, England, 2004).

[8] C. Nisoli, N. M. Gabor, P. E. Lammert, J. D. Maynard, and V. H. Crespi, Phys. Rev. Lett. **102**, 186103 (2009).

[9] L. S. Levitov, Phys. Rev. Lett. **66**, 224 (1991); EPL **14**, 533 (1991).

[10] A. W. Thompson, *On Growth and Form* (Cambridge University Press, New York, 1959) (first edition, 1917); R. V. Jean, *Phyllotaxis: A Systemic Study in Plant Morphogenesis* (Cambridge University Press, Cambridge, England, 1994).

[11] I. Adler, D. Barabe, and R. V. Jean, Ann. Bot. (London) **80**, 231 (1997).

[12] A. Frey-Wyssling, Nature (London) **173**, 596 (1954); R. O. Erickson, Science **181**, 705 (1973).

[13] N. Rivier, R. Occelli, J. Pantaloni, and A. Lissowski, J. Phys. (France) **45**, 49 (1984).

[14] P. M. Chaikin and T. C. Lubensky, *Principles of Condensed Matter Physics* (Cambridge University Press, New York, 2000).

[15] C. Nisoli *et al.* (unpublished).

[16] A. Rahman and J. P. Schiffer, Phys. Rev. Lett. **57**, 1133 (1986); J. P. Schiffer, *Proceedings of the Particle Accelerator Conference* (IEEE, Piscataway, NJ, 1995) Vol. 5, p. 3264.

[17] T. Schätz, U. Schramm, and D. Habs, Nature (London) **412**, 717 (2001); U. Schramm, T. Schatz, and D. Habs, Phys. Rev. E **66**, 036501 (2002).

[18] D. J. Pochan *et al.*, Science **306**, 94 (2004).

[19] Y. Choi, K. Kim, and H. K. Pak, Physica A **281**, 99 (2000).

[20] K. J. Strandburg, Rev. Mod. Phys. **60**, 161 (1988).